Journal of Membrane Science 493 (2015) 755–765

Contents lists available at ScienceDirect

Journal of Membrane Science

journal homepage: www.elsevier.com/locate/memsci

Zwitterionic copolymer self-assembly for fouling resistant, high flux membranes with size-based small molecule selectivity

Prity Bengani, Yangming Kou, Ayse Asatekin*

Department of Chemical and Biological Engineering, Tufts University, 4 Colby Street, Medford, MA 02155, USA

ARTICLE INFO

Article history:
Received 7 April 2015
Received in revised form
26 June 2015
Accepted 13 July 2015
Available online 20 July 2015

Keywords:
Self-assembly
Zwitterion
Sulfobetaine
Fouling
Membrane

ABSTRACT

Membranes that exhibit size-based rejection between small molecules (< 1500 g/mol) independent of solute charge would be valuable for many separations, but commercial membranes show poor and unpredictable selectivity at this size range. This arises from high pore size polydispersity and charged membrane surfaces that lead to separations affected by solute charge. Furthermore, these membranes are susceptible to fouling. Self-assembly is a promising technique for making polymeric membranes with fouling resistance, high permeability and selectivity along with opportunity for easy fabrication and scalability. We report the first examples of a new class of membrane materials that derive their permeability, size-based selectivity and fouling resistance from the self-assembly of zwitterion-containing amphiphilic random copolymers. Zwitterionic groups strongly resist biomacromolecular fouling due to their high affinity with water, and self-assemble into channel-type clusters of 0.6–2 nm in size. We show that these copolymers self-assemble into bicontinuous nanodomains. Thin film composite membranes formed by coating these copolymers onto porous supports exhibit permeances as high as 8.4 L m^{-2} h^{-1} bar^{-1}, over three times that of a commercial membrane with similar MWCO. They show size-based selectivity, with a cut-off around 1 nm. This closely matches the size of zwitterionic domains measured by transmission electron microscopy, indicating permeation occurs through these self-assembled "nanochannels." These membranes show excellent fouling resistance during filtration of protein solutions and oil emulsions, completely resisting irreversible fouling and retaining over 96% of their permeance during filtration. These membranes have potential uses in biomolecule separations, purification of pharmaceuticals, and wastewater treatment.

1. Introduction

Membrane filtration is a green separation method with numerous applications in the production of biochemicals, pharmaceuticals [1], food industry, and water treatment [2,3]. They are an energy efficient, environmentally friendly and scalable separation method in comparison with conventional processes like distillation and chromatography. To achieve wider use, better membranes are needed that are capable of performing useful separations by providing selectivity between desired components while exhibiting ease of manufacturing, high flux and resistance to fouling, described as the loss of membrane permeability due to the adhesion of feed components on the membrane surface [3–7].

Membranes that exhibit size-based selectivity between small molecules (< 1500 g/mol) independent of solute charge would be valuable for many separations, especially in the manufacture and purification of peptides and other low molecular weight biopharmaceuticals [1,8] and nutraceuticals [9]. However, this remains an area where very few commercial membranes are available. Ultrafiltration (UF) membranes are typically defined as membranes with effective pore sizes in the 2–100 nm range [3]. They separate solutes based on size, but they are often limited to retaining and separating macromolecular solutes such as proteins. The few commercial UF membranes with nominal molecular weight cut-off (MWCO) < 5000 Da often suffer from high pore size polydispersity. They are also often negatively charged to prevent fouling [3,5,10], which affects rejection. Nanofiltration (NF) membranes, designed for retaining doubly charged ions [3,11], have reported pore sizes in the right range (1–3 nm), but their true basis of separation is a hybrid between pore flow and solution–diffusion mechanisms [3]. Rejection is strongly affected by not only solute size but also charge and chemical interactions. Neither UF nor NF membranes that are currently commercially available exhibit predictable size-based selectivity.

* Corresponding author.
E-mail addresses: prity.bengani@tufts.edu (P. Bengani), yangming.kou@tufts.edu (Y. Kou), ayse.asatekin@tufts.edu (A. Asatekin).

http://dx.doi.org/10.1016/j.memsci.2015.07.025
0376-7388/

Other researchers have prepared membranes with ~1 nm pores by narrowing the pores of track-etched membranes by electroless gold deposition [12], molecular "squares" coated onto a porous substrate to form thin film composite (TFC) membranes [13], and lyotropic liquid crystal (LLC) assemblies [14–16]. Although these membranes have pore sizes in the right range, they suffer from one or more limitations. Most exhibit low flux, and their fouling performance was not reported. LLC-based membranes have charged surfaces, and hence have selectivity that is strongly affected by solute charge [14–16]. Others are difficult and expensive to manufacture at large scale [17–19].

Polymer self-assembly, which allows spontaneous formation of nano-scale structures, is a promising tool for scalable manufacture of membranes with controlled pore size and sharp selectivity while maintaining high permeability [4,20–25]. Block copolymer (BCP) self-assembly is documented to make membranes with high-density uniformly sized pores using a bottom-up approach [4,20,26], but requires tightly-controlled processing conditions. It is also limited to pore sizes that can be achieved by BCP self-assembly, above 3 nm [27]. As an alternative, Mayes and coworkers have used comb-shaped copolymers with hydrophobic backbones and hydrophilic poly(ethylene oxide) (PEO) side-chains, which self-assemble to form bicontinuous microphases [21–24,28,29]. The hydrophilic phase acts as a network of nanochannels, ~1–2 nm in diameter. They have reported membranes with sub-nanometer size selectivity and good antifouling capability. But there are concerns regarding PEO stability in oxidizing environments [30,31] such as during in situ sterilization of filtration systems in the biopharmaceutical and food industries. This narrows the applications these membranes can be used in.

Zwitterions, defined as neutral molecules with equal numbers of positively and negatively charged functional groups, offer an alternative and robust fouling resistance chemistry. They have been shown to be highly resistant to biomolecular fouling due to their high degree of hydration [32–37]. Since this discovery, many researchers have improved the fouling resistance of membranes by attaching zwitterionic groups on their surface, by post-processing existing membranes [38–44] or by using zwitterionic surface-segregating additives [45–47]. Two studies incorporated zwitterionic groups in charged hydrogel layers to boost fouling resistance [48,49]. However, amphiphilic zwitterionic copolymers have not been explored as membrane selective layers themselves. The self-assembly of zwitterionic groups is unexplored as a tool to create membrane selective layers with tunable, controlled selectivity in addition to fouling resistance.

Most studies on how zwitterionic amphiphiles self-assemble center on simulation studies and micellization of zwitterionic surfactants. Typical dipole moments of sulfobetaine-type zwitterions are ~18.7–27.6 D [50], whereas water is only 1.9 D. Due to the presence of permanent dipoles and large electrostatic attractions, antiparallel arrangement of dipoles is theoretically predicted to be the most energetically favorable, and the formation of tubular (channels) or lamellar (disk-like) structures are suggested to be strongly favored, as opposed to spheres [34,51]. Studies on the self-assembly of zwitterionic amphiphilic copolymers indicate that zwitterions form clusters ~1–5 nm in size, as measured by small angle X-ray studies and solid state NMR, but do not report morphology [52–58]. The self-assembly is driven by the strong dipole–dipole interactions between the zwitterionic groups, as well as the differences in χ parameter between the hydrophobic and zwitterionic repeat units [52–59].

Based on these studies, we would expect the morphology of zwitterionic amphiphilic random copolymers to comprise a bicontinuous network of channel-like domains of zwitterions, with their dipoles in anti-parallel orientation, held together by the hydrophobic domains (Fig. 1a). We aim to use this hypothesis as a guideline to rationally design polymers for the explicit purpose of creating a self-assembled structure that will lead to the desired membrane properties: permeability, selectivity, and fouling resistance. We hypothesize that the zwitterionic, easily hydrated domains can act as a bicontinuous network of "nanochannels" suitable for solute and water permeation, held together by the hydrophobic "channel walls." This would make these polymers promising materials for membrane selective layers that derive their selectivity and permeability from this self-assembled nanostructure. The bicontinuous morphology leads to high permeability with easy processing, without any need for alignment. The hydrophobic component is selected to be rigid and glassy to prevent swelling of the zwitterionic nanochannels that would otherwise lead to the loss of selectivity and integrity when exposed to water. The selectivity would be determined by zwitterionic domain size, expected to be ~1 nm. Finally, due to the presence of zwitterionic groups, we expect these membranes to be highly fouling resistant.

In this study, we report the first examples of this new class of high flux, fouling resistant membranes with ~1 nm effective pore size that feature self-assembling zwitterionic amphiphilic random

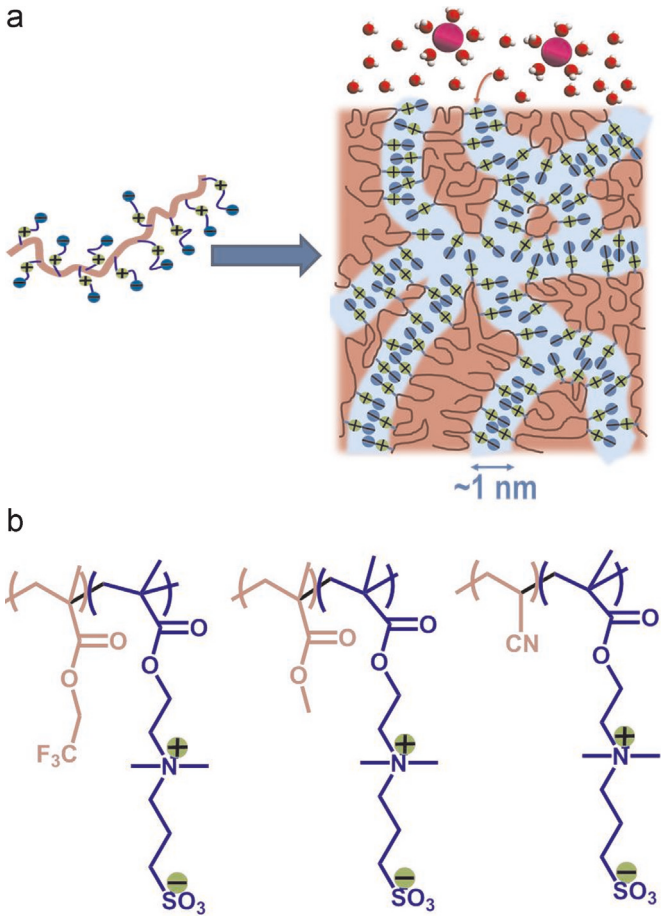

Fig. 1. Self-assembly of zwitterionic copolymers leading to the formation of effective "nanochannels" permeable to water and solutes. a. Schematic of the copolymer (left) undergoing self-assembly to form the proposed nanostructure (right) featuring bicontinuous networks of zwitterionic (indicated by green and blue charged groups) and hydrophobic (pink) domains. The zwitterionic domains act as a network of hydrophilic nanochannels ~1 nm in diameter, held together by the glassy hydrophobic domains. Water molecules and solutes smaller or equal to the domain size (red) can enter these channels and permeate through the membrane, while larger solutes (fuchsia) are retained. b. Chemical structures of the copolymers – PTFEMA-*r*-SBMA, PMMA-*r*-SBMA, and PAN-*r*-SBMA (left to right). (For interpretation of the references to color in this figure legend, the reader is referred to the web version of this article.)

copolymers as their selective layer, designed based on the above hypothesis. We document the self-assembled morphology of amphiphilic random copolymers with glassy backbones and sulfobetaine side-groups imaged by transmission electron microscopy (TEM). Membranes whose selective layers are composed of these copolymers show a sharp cut-off based on solute size, independent of solute charge, that closely correlates with the zwitterionic domain spacing, around 1 nm. We also demonstrate the excellent fouling resistance of these membranes.

2. Experimental

2.1. Materials

Sulfobetaine methacrylate (SBMA), azobisisobutyronitrile (AIBN), 4-methoxy phenol (MEHQ), bovine serum albumin (BSA, 66.5 kDa), methyl methacrylate (MMA), acrylonitrile (AN), and lithium chloride (LiCl) were purchased from Sigma Aldrich (St. Louis, MO). 2,2,2 Trifluoroethyl methacrylate (TFEMA) was obtained from Scientific Polymer Products Inc (Ontario, NY). Trifluoroethanol (TFE), basic activated alumina, dimethyl sulfoxide (DMSO), methanol (MeOH), ethanol, isopropanol, hexane, tetrahydrofuran (THF), copper (II) chloride ($CuCl_2$), and cesium chloride (CsCl) were purchased from VWR (West Chester, PA). Deuterated dimethyl sulfoxide (DMSO-d_6) and deuterium oxide (D_2O) were obtained from Cambridge Isotope Laboratory (Tewksbury, MA). DC193 surfactant was obtained from Dow Chemicals (Providence, RI). All chemicals and solvents were reagent grade and used as received, except TFEMA, AN and MMA monomers, which were purified by passing through a basic activated alumina column. PVDF 400R ultrafiltration membranes purchased from Sepro Membranes Inc. (Oceanside, CA) were used as the base membrane for our polymer coatings. Poly(ether sulfone) (PES) 1000 molecular weight cut-off (MWCO) membranes (Sartorius) purchased from Fisher Scientific Inc (Pittsburgh, PA) were used as control. Ultrapure deionized water generated by Biolab 3300 RO, a building-wide RO/DI water purification unit by Mar Cor Purification was used for all the experiments.

2.2. Synthesis of zwitterionic amphiphilic copolymers

2.2.1. Synthesis of PTFEMA-r-SBMA copolymers

SBMA was dissolved in dimethyl sulfoxide using approximately 20 ml of DMSO per gram of SBMA in a round-bottomed flask. TFEMA was passed through a column of basic activated alumina to remove the inhibitor and added to the flask, totaling 10 g of monomer mixture, followed by 0.01 g of azobisisobutyronitrile. The flask was sealed with a rubber septum, purged with nitrogen gas and placed in an oil bath at 70 °C. The reaction was allowed to run for at least 20 h. 0.5 g of 4-methoxyphenol was added to the flask to terminate the reaction. Copolymers with an SBMA content of ~50% were precipitated in a 50:50 mixture of THF and MeOH. Copolymers with a higher SBMA content (>50%) were precipitated in methanol, while those with lower amount of SBMA were precipitated in a 50:50 mixture of ethanol and hexane. In each case, the precipitate was vacuum filtered, extracted with methanol twice for at least 8 h to remove remaining solvent and monomers. The final product was dried in the vacuum oven overnight at 50 °C. The copolymer composition was determined by ^{1}H-NMR spectroscopy.

2.2.2. Synthesis of PMMA-r-SBMA and PAN-r-SBMA copolymers

PMMA-*r*-SBMA and PAN-*r*-SBMA were also synthesized by free radical polymerization using an analogous procedure. 5 g of SBMA was dissolved in dimethyl sulfoxide using approximately 20 ml of DMSO per gram of SBMA in a round-bottomed flask. 5 g of MMA (or AN) was passed through a column of basic activated alumina to remove the inhibitor and added to the flask, totaling 10 g of monomer mixture, followed by 0.01 g of AIBN. The flask was sealed with a rubber septum, purged with nitrogen gas and placed in an oil bath at 70 °C. Reaction was allowed to run for at least 20 h. 0.5 g of 4-methoxyphenol was added to the flask to terminate the reaction. Copolymers were precipitated in methanol, the precipitate was vacuum filtered, extracted with methanol twice for at least 8 h to remove remaining solvent and monomers. The final product was dried in the vacuum oven overnight at 50 °C. The copolymer composition was determined by ^{1}H-NMR spectroscopy.

2.3. Characterization of PTFEMA-r-SBMA copolymers

2.3.1. Molecular weight

In order to estimate the molecular weight of these copolymers, we performed dynamic light scattering (DLS) (Brookhaven Instruments Nanobrook ZetaPALS). A 35 mW red diode laser with a nominal wavelength of 659 nm was used as the light source. All the measurements were done on copolymer solutions in TFE at a concentration of 1 mg/ml at a scattering angle of 90° and a temperature of 25 °C, which was controlled by means of a thermostat. A 0.2 μm filter was used to remove dust before light scattering experiments. After stabilization of samples for two minutes, three measurements were performed for each copolymer ratio. The effective hydrodynamic radius and relative molecular weight based on polyacrylonitrile standards in dimethyl formamide (DMF) were determined by the instrument software (BIC Particle Solutions v. 2.5).

2.3.2. Self-assembled nanostructure

To characterize the morphology of the self-assembled structure of PTFEMA-*r*-SBMA, we used transmission electron microscopy (TEM). TEM images were obtained by FEI Technai Spirit in bright field mode operated at 80 keV. Copolymer films were cast from 10% (w/v) trifluoroethanol (TFE) solution into Teflon dishes. To enhance contrast, zwitterionic domains were positively stained with 2% aqueous copper (II) chloride ($CuCl_2$) solution for 4 h. $CuCl_2$ was chosen because sulfobetaine and copper form stable complexes [61]. Similar images for P50 copolymer were observed by staining with cesium chloride (CsCl), but Cs seemed to form clusters of dark regions instead of homogeneous staining, and hence was not as suitable as $CuCl_2$. Stained films were embedded in EMbed 812 epoxy resin for two nights with frequent epoxy replacement, and ultrathin ~50 nm sections cut using an ultramicrotome were placed on copper grids (200 mesh, Electron Microscopy Sciences). TEM acquisition was performed by Dr. Nicki Watson at W. M. Keck foundation Biological Imaging Facility at the Whitehead Institute. Fast Fourier Transform analysis was performed on the TEM images using ImageJ software.

To measure water uptake, solvent-cast films of PTFEMA-*r*-SBMA, approximately 50 mg in mass, were weighed in their dry state. They were then immersed in deionized water for 24 h. The samples were removed, dabbed with a lint-free wipe to remove water on the surface, and reweighed. Water uptake (wt%) was calculated from the difference between the two measurements divided by the dry weight.

2.4. Preparation of thin film composite membranes

Copolymers were dissolved in TFE at 50 °C to make a 10% w/v solution. The resulting solution was passed through a 1 μm glass fiber syringe filter (Whatman) and degassed by heating to 50 °C in a sealed vial for at least an hour until no gas bubbles were visible. Solution was brought to room temperature and thin film

composite membranes were formed by coating onto PVDF 400R ultrafiltration membrane (Sepro membranes, Oceanside, CA) with a doctor blade set at a gate size of 25 μm. The membrane was immersed immediately in a bath of isopropanol for 20 min, followed by deionized water at least overnight.

2.5. Characterization of membrane morphology

Membrane thickness and morphology was characterized by using Phenom G2 Pure Tabletop Scanning electron microscopy (SEM) operating at 5 kV. Membrane samples were freeze-fractured using liquid nitrogen for cross-sectional examination, and sputter coated with gold-palladium before imaging.

2.6. Characterization of membrane performance

Filtration experiments were performed on 25 mm diameter membranes using a 10 ml Amicon 8010 stirred, dead-end filtration cell (Millipore) with an effective filtration area of 4.1 cm^2, attached to a 1 gal reservoir. All filtration experiments were performed by applying a transmembrane pressure of 20 psi (1.4 bar). Filtration cells were continuously stirred using a stir plate to minimize concentration polarization. Deionized water was first passed through the membrane until the flux remained stable over at least 30 min. Upon stabilization, permeate was collected at 15 min intervals for an hour, and weighed to determine the transmembrane flux. Flux is the flow rate through the membrane normalized by membrane area. Permeance is a membrane property that normalizes the flux to account for the applied transmembrane pressure difference, and is obtained by

$$L_p = \frac{J}{\Delta p} = \frac{1}{R_{total}} \quad (1)$$

Where L_p is the permeance of the membrane ($L\,m^{-2}\,h^{-1}\,bar^{-1}$), J is the water flux across the membrane ($L\,m^{-2}\,h^{-1}$), Δp is the trans-membrane pressure (bar), and R_{total} is the resistance of the TFC membrane to flow ($L^{-1}\,m^2\,h^1\,bar^1$). To account for the hydraulic resistance posed by the support membrane, we used the resistance-in-series model. Having obtained the permeance of the thin film composite membrane, we calculated total resistance to flow using Eq. (1). The permeance of the uncoated PVDF 400R base membrane was experimentally measured and found to be 1340 $L\,m^{-2}\,h^{-1}\,bar^{-1}$. We calculated the resistance provided by the uncoated membrane by taking the inverse of its permeance. We obtained the copolymer coating resistance using

$$R_{coating} = R_{total} - R_{support} \quad (2)$$

Where R_{total} is membrane's total resistance ($L^{-1}\,m^2\,h^1\,bar^1$), $R_{support}$ is the resistance of the uncoated support membrane ($L^{-1}\,m^2\,h^1\,bar^1$), and $R_{coating}$ is the resistance of the copolymer coating ($L^{-1}\,m^2\,h^1\,bar^1$). From the coating resistance we obtained coating permeance. Finally, we calculated membrane permeability by normalizing the permeance with coating thickness, defined as

$$P_m = L_p\delta = \frac{\delta}{R_{coating}} \quad (3)$$

Where P_m is the membrane permeability ($L\,\mu m\,m^{-2}\,h^{-1}\,bar^{-1}$) and δ is the membrane thickness (μm). For each copolymer ratio, at least three membrane samples from the same sheet were tested.

To characterize the selectivity of our membranes, we filtered a series of dyes and vitamins of various sizes. A 100 mg/L aqueous solution of solute was filtered through the membrane. In case of filtering solute mixtures, the total concentration was kept fixed at 100 mg/L. The first ml of filtrate was discarded, and the subsequent 1–2 ml of filtrate was used to calculate rejection, which is defined as

$$R = \frac{100\,(C_f - C_p)}{C_f} \quad (4)$$

Where R is the solute rejection (%), C_f is the feed concentration (mg/L), and C_p is the permeate concentration (mg/L). Solute concentration in the feed and permeate were measured by UV–vis spectroscopy (Thermo Scientific Genesys 10S). For each copolymer ratio, two membrane samples from the same sheet were tested.

Fouling tests were performed using the same equipment but a slightly different setup for flux measurement. A Scout Pro SP401 balance connected to a Dell laptop was used to automatically measure the permeate weight every 30 s using TWedge 2.4 software (TEC-IT, Austria). The permeate flow occurs one droplet at a time; hence the measured volume at each data point can vary by 1–2 droplets amounting to 0.05–0.1 ml. Two separate experiments of 1500 mg/L oil-in-water emulsion (9:1 ratio of soybean oil: DC193 surfactant) [62] and 1 g/L of Bovine serum albumin in PBS buffer (pH 7.4) were performed. First deionized water was filtered through the membrane until the flux stabilized. This was taken as the zero time point in the plots. The cell and reservoir were filled with the foulant solution. After filtering the foulant solution for the selected time period, the cell was rinsed several times with DI water and refilled with DI water to determine the reversibility of fouling. Same procedure was followed for both foulants and for zwitterionic membranes as well as controls. Protein concentration in feed and permeate was quantified using UV absorbance at 280 nm. The permeate after filtering oil emulsions (gray) appeared clear indicating retention of oil droplet components, and was not further quantified.

2.7. Characterization of membrane stability

In order to confirm the stability of the membrane upon chlorine exposure, samples were soaked in aqueous solution of sodium hypochlorite at a concentration of 1000 ppm, adjusted to pH 7.1 by the addition of small amounts of concentrated HCl, for three hours. Chlorine solution was freshly prepared and the concentration of free chlorine in the solution was confirmed using chlorine test strips. After soaking in chlorine, the membrane was thoroughly rinsed with water several times. To evaluate membrane performance, water permeance and retention of one of the dyes right around the cut-off (Chicago Sky Blue 6B) was measured before and after soaking as described in Section 2.6.

3. Results and discussion

3.1. Synthesis of zwitterionic amphiphilic copolymers

We have synthesized statistical copolymers of sulfobetaine methacrylate (SBMA), a zwitterionic monomer, with three relatively hydrophobic monomers: acrylonitrile (AN), 2,2,2-trifluoroethyl methacrylate (TFEMA), and methyl methacrylate (MMA) (Fig. 1b). The monomers were selected to have homopolymer glass transition temperatures significantly above room temperature (74 °C for PTFEMA, 100 °C for PAN, 110 °C for PMMA) so that the material would remain rigid even upon the hydration of the zwitterionic groups. Free radical copolymerization was used due to its robustness and scalability. Fig. 2 shows the reaction scheme for the free radical polymerization of PTFEMA-*r*-SBMA copolymers. Other copolymers were synthesized by analogous reaction schemes.

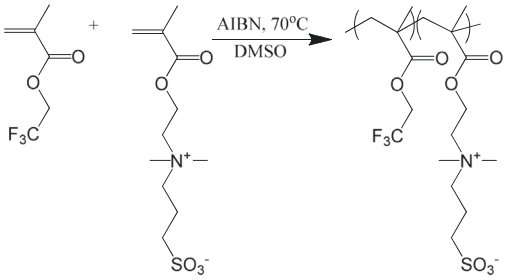

Fig. 2. Schematic showing the synthesis of PTFEMA-*r*-SBMA copolymer using free radical polymerization of TFEMA (left) and SBMA (right) monomers.

All three copolymers were synthesized successfully (Fig. 3). PTFEMA-*r*-SBMA copolymers with SBMA contents ranging between 30 and 70 wt% were synthesized. Conversion at the end of the reaction period was ~70%. Copolymer composition was characterized by ^{1}H-NMR (Bruker Avance III 500 MHz) using 1% LiCl in deuterated DMSO. Sample spectra and peak assignments for the three polymers are given in Fig. 3.

PTFEMA-*r*-SBMA copolymer compositions were found to be within ~5% of monomer composition in the reaction mixture (Table 1), indicating that copolymerization was essentially random [63]. ^{1}H-NMR showed that PAN-*r*-SBMA synthesized from a monomer mixture containing 50 wt% SBMA contained 52 wt% SBMA, essentially identical to the monomer composition in the reaction mixture. PMMA-*r*-SBMA, also synthesized from a monomer mixture with 50 wt% SBMA, was slightly enriched in MMA, and contained 42 wt% SBMA. While only one monomer ratio was tested for these copolymers, the fact that SBMA is not highly enriched in the copolymer indicates that large SBMA blocks are not likely to be present. All three copolymers are white and glassy, and soluble in dimethyl sulfoxide, trifluoroethanol and formamide. After initial screening, PTFEMA-*r*-SBMA copolymers were found to show better processability for membrane manufacture. Therefore, additional compositions of PMMA-*r*-SBMA and PAN-*r*-SBMA were not prepared for this study.

3.2. Characterization of PTFEMA-r-SBMA copolymers

3.2.1. Characterization of molecular weight

To estimate the molecular weight of PTFEMA-*r*-SBMA copolymers, we performed dynamic light scattering (DLS) on 1 mg/ml solutions of the copolymers in trifluoroethanol. P50, P40 and P30 copolymers had effective hydrodynamic radii of 33.3 ± 0.11 nm, 30.3 ± 0.5 nm, and 34.9 ± 1.9 nm, respectively. These were converted to relative molecular weights calculated by the software Brookhaven Particle Solutions v. 2.5 based on an internal database of standards (polyacrylonitrile standards in dimethyl formamide). These radii were found to correspond to a molecular weight of 1.37×10^6 g/mol, 1.19×10^6 g/mol, and 1.65×10^6 g/mol for P50, P40 and P30 copolymers respectively. It should be noted that these molecular weights are relative values of polymer chains of equivalent hydrodynamic radius. These results are affected by polymer chains aggregating in solution, and is highly dependent on polymer–solvent interactions [60]. Nevertheless, it provides valuable information about an order-of-magnitude estimate of molecular weight. The large relative molecular weights indicate that the copolymers are also long chains, likely above the entanglement molecular weight.

3.2.2. Characterization of the self-assembled morphology

To characterize the morphology of the self-assembled structure of PTFEMA-*r*-SBMA copolymers, we used TEM. Zwitterionic domains were preferentially stained by immersion into 2% aqueous

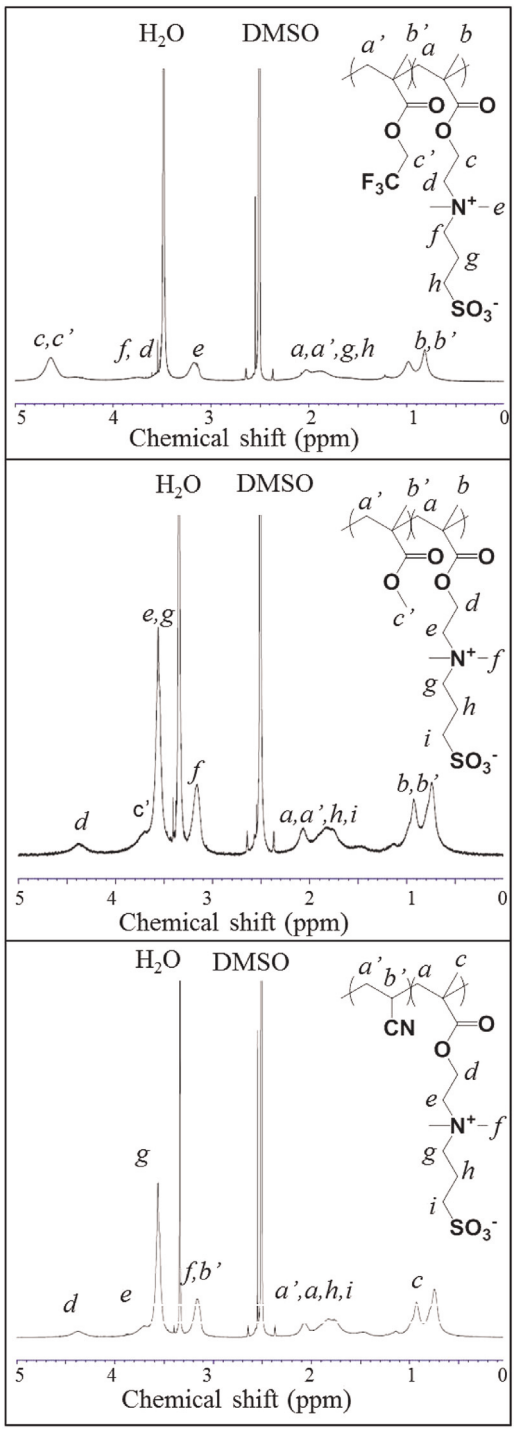

Fig. 3. ^{1}H-NMR spectra of amphiphilic zwitterionic copolymers. Plots indicate successful copolymerization of PTFEMA-*r*-SBMA (top), PMMA-*r*-SBMA (middle), and PAN-*r*-SBMA (bottom) with an SBMA content of 25%, 42% and 52% respectively by weight.

$CuCl_2$ solution, relying on the formation of stable complexes between sulfobetaine and copper [61]. Fig. 4 shows bright field TEM images of PTFEMA-*r*-SBMA copolymers with 47 wt% (P50) and 25 wt% (P30) SBMA. P50 shows bicontinuous networks with both TFEMA and SBMA. This self-assembled structure has similarities with those reported for Nafion [64], which is also a copolymer with a fluorine-containing backbone and highly polar side-groups. The dark areas (stained SBMA domains) were measured to be 48%

Table 1
Composition of PTFEMA-*r*-SBMA copolymers used in this study.

Polymer code	SBMA content in monomer mixture (wt%)	SBMA content in PTFEMA-*r*-SBMA (wt%)[a]	Water uptake[b] (%)
P50	50	47	37.1
P40	40	36	26.9
P30	30	25	0.6

[a] Determined by ^{1}H NMR spectroscopy.
[b] Solvent-cast polymer films soaked in water for 24 h.

of the total area (Image J), consistent with the copolymer composition. The domain periodicity of ~2.4 nm/cycle was determined from the fast fourier transform (FFT) image, corresponding to a domain size of ~1.2 nm. In contrast, P30 shows sparsely packed, less interconnected zwitterionic domains surrounded by large hydrophobic (white) regions, with the dark areas corresponding to 27% of the total area. Decreasing the zwitterionic content seems to visibly affect the copolymer morphology. Due to low zwitterionic content in the P30 copolymer, the stain was seen to penetrate the sample less effectively, accumulating on the surface of the film at the interface with the epoxy, as observed in Fig. 4c. Therefore, an accurate channel size cannot be obtained from this image. Nevertheless, it is still possible to conclude that copolymers with zwitterionic content less than or equal to P30 (25 wt%) do not have sufficient SBMA to form an interconnected network of channels that percolates through the thickness of the film.

These results are also supported by the amount of water uptake when copolymer pieces were soaked in water for 24 h (Table 1). Water uptake is found to be closely correlated with the zwitterionic content in the copolymer. P50 and P40 copolymers took up 37 and 27 wt% of water, while P30's weight change was negligible. This suggests that at low zwitterion contents, water is not able to effectively penetrate the copolymer due to the poor interconnectivity between zwitterionic domains. Conversely, copolymers with SBMA contents 60 wt% and above would swell extensively, disintegrate and partially or fully dissolve in water. This indicates that there is a copolymer composition range that amphiphilic zwitterionic copolymers can operate as permeable membrane selective layers.

3.3. Preparation of thin-film composite membranes

To study membranes whose selective layers are made of these copolymers, we prepared thin film composite membranes by coating commercially available ultrafiltration support membranes with the copolymer dissolved in trifluoroethanol (TFE) using a doctor blade and immersing in isopropanol to quickly precipitate the polymer. We achieved TFC membranes with dense coating layers of PTFEMA-*r*-SBMA ~1 μm in thickness as seen under a Scanning Electron Microscope (SEM), except for the P30-coated membrane (Fig. 5). Coatings made from P30 were asymmetric, with a thin non-porous skin supported by a porous copolymer layer on top of the support membrane. Dense versus porous coatings are attributed to the differences in solvent/non-solvent diffusivity and solvent/non-solvent quality for the various copolymer compositions [3]. Since PTFEMA-*r*-SBMA copolymers showed better processability for membrane manufacture, we focused most of our studies on them. Membranes with PAN-*r*-SBMA, and PMMA-*r*-SBMA were prepared in a similar fashion and will be discussed later on in Section 3.4.2.2.

3.4. Characterization of PTFEMA-r-SBMA TFC membrane performance

3.4.1. Water permeability

To characterize the membrane performance, we performed dead-end stirred cell filtration experiments with deionized (DI) water applying a transmembrane pressure of 20 psi (1.4 bar).

P50 and P40-coated membranes showed high water permeances, up to 8.4 L m^{-2} h^{-1} bar^{-1} (Table 2). We selected a commercial membrane with a similar size cut-off as ours as a control, a poly(ether sulfone) (PES) membrane with a reported nominal molecular weight cut-off (MWCO) of 1 kDa (Sartorius). The water permeance of this membrane was 2.55 ± 0.1 L m^{-2} h^{-1} bar^{-1}, significantly lower than P40-coated and P50-coated membranes.

Water permeance of TFC membranes depends strongly on selective layer thickness. Most reverse osmosis (RO) and nanofiltration (NF) TFC membranes have selective layer thicknesses as low as 0.1 μm, much thinner than those of the TFC membranes described here. With optimized coating methods to reduce the selective layer thickness, even higher permeances can be achieved. To account for the effect of selective layer thickness, we obtained the water permeability of the synthesized copolymers as described earlier. An accurate permeability could not be calculated for P30 as the coated membrane had a porous selective layer. We calculated the permeabilities of P50 and P40 selective layers to be 10.5 and 6.9 L μm m^{-2} h^{-1} bar^{-1} respectively. In comparison, selective layer permeabilities of RO and NF membranes are in the range 0.047–0.28 L μm m^{-2} h^{-1} bar^{-1} and 0.3–1.8 L μm m^{-2} h^{-1} bar^{-1}, respectively [65]. This indicates that the PTFEMA-*r*-SBMA

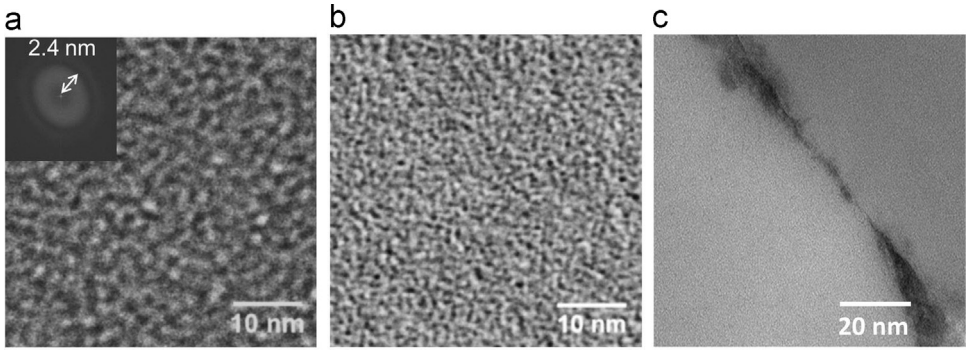

Fig. 4. TEM bright field images of the self-assembled morphology of PTFEMA-*r*-SBMA copolymers with different SBMA contents. Zwitterionic SBMA domains were stained with Cu^{2+} ions and appear dark. PTFEMA phase forms the lighter regions. Inset shows Fast Fourier Transform of the image, with the characteristic period indicated on the arrow. a. TEM image for P50, containing 47 wt% SBMA, shows interconnected SBMA domains with a characteristic period of ~2.4 nm, yielding a channel size around 1.2 nm. b. TEM image for P30, containing 25 wt% SBMA, exhibits sparsely packed, less interconnected SBMA domains. c. TEM of the interface between the P30 copolymer and epoxy, showing uneven penetration and accumulation of stain on the outer surface of the microtomed sample.

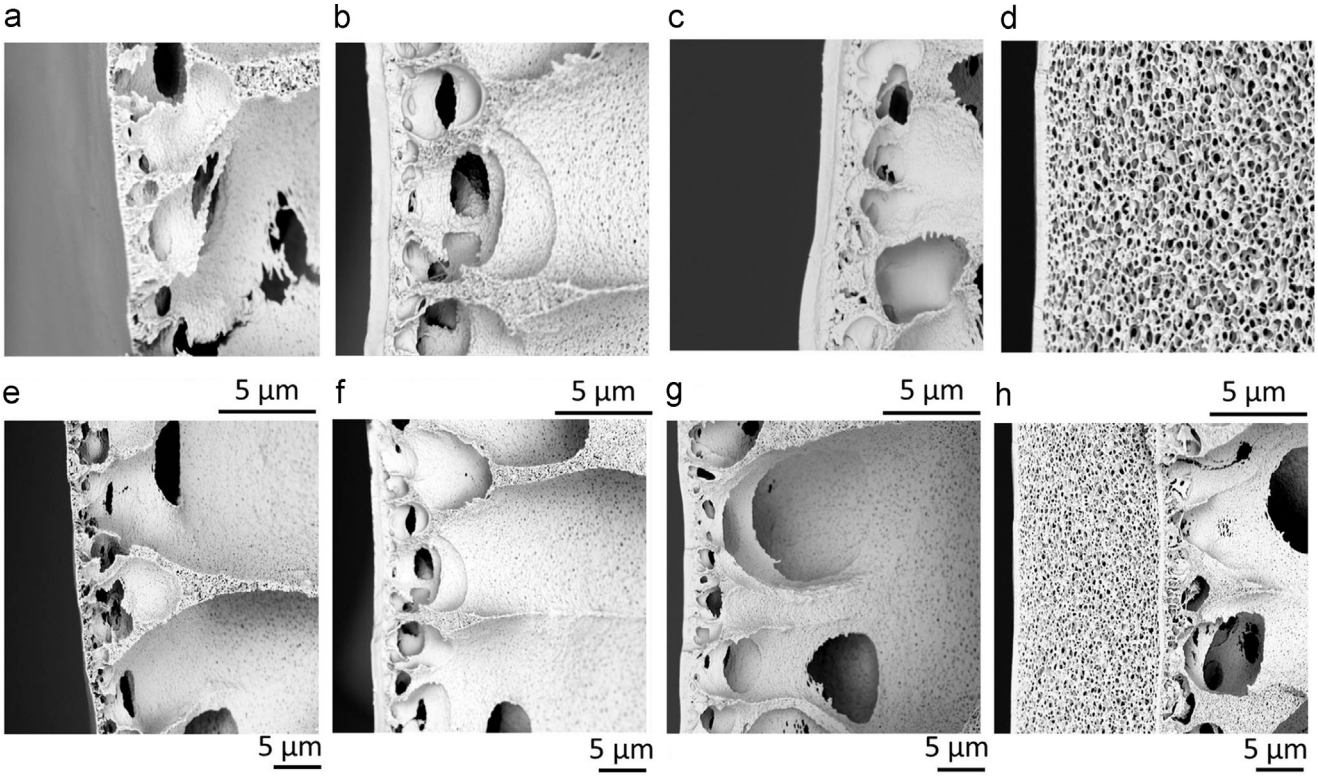

Fig. 5. Cross-sectional SEM images of uncoated support membrane, and thin film composite (TFC) membranes with PTFEMA-*r*-SBMA selective layers with varying SBMA contents. (a,e) Uncoated support membrane (PVDF 400R). (b,c,d,f,g,h) TFC membranes made by coating the support membrane with (b,f) P50 (c,g) P40 (d,h) P30. P50 and P40 coated membranes show a dense ~1 μm copolymer coating, while the coating made of P30 shows a thin, dense selective layer at the surface of a porous copolymer layer. (a, b,c,d) 10,000× magnification, (e,f,g,h) 5000× magnification.

Table 2
DI water permeance and permeability of PTFEMA-*r*-SBMA thin film composite (TFC) membranes in comparison to a commercial membrane of similar pore size.

Membrane coating material	Permeance ($L\,m^{-2}\,h^{-1}\,bar^{-1}$)	Coating thickness (μm)	Permeability[b] ($L\,\mu m\,m^{-2}\,h^{-1}\,bar^{-1}$)
P50	8.4 ± 0.35	1.25 ± 0.31	10.5 ± 0.45
P40	5.9 ± 0.15	1.16 ± 0.06	6.9 ± 0.15
P30	0.33 ± 0.03	21.4 ± 6.84	Porous layer
PES 1 kDa[a]	2.55 ± 0.1	N/A	N/A

[a] Commercial membrane (Sartorius).
[b] Calculated using resistance in series model.

copolymers with at least 36 wt% SBMA show significantly higher permeabilities than commercial NF and RO selective layers.

P50 copolymer permeability was 54% higher than that of P40, showing that the copolymer permeability is directly proportional to the SBMA content (wt%) for these two. This indicates that the effective porosity, or the volume fraction of nanochannels, is directly proportional to the zwitterionic monomer content. In contrast, P30-coated membrane showed very low permeance despite its very thin non-porous selective layer, in agreement with the poor interconnectivity between zwitterionic domains observed by TEM.

3.4.2. Membrane selectivity

A crucial property of membranes is their selectivity. Based on our hypothesis, we would expect our membranes to exhibit size-based selectivity with an effective pore size comparable to this measured domain size, ~1 nm. Since these copolymers are electrostatically neutral overall, their selectivity should not be affected by solute charge. Hence, TFC membranes whose selective layers are composed of the proposed copolymers are expected to have size-based selectivity, with a cut-off around 1 nm. This corresponds to a molecular weight cut-off on the order of 1000 g/mol [66]. To characterize membrane selectivity, we performed dead-end stirred cell filtration experiments with a series of small organic molecules. We selected negatively charged dyes and vitamins with overall neutral charge (Table 3), because these are rigid molecules whose sizes are comparable with the measured domain size. Molecular diameters were calculated by determining the molecular volume of the solute using Molecular Modeling Pro (ChemSW) and calculating the diameter of a sphere of equivalent volume [21,23,29].

3.4.2.1. Effect of zwitterionic content in the copolymer. Fig. 6a shows the rejection of negatively charged dyes through P50, P40 and P30-coated membranes. These membranes exhibit sharp selectivity with a size cut-off around 0.8 – 1 nm, essentially independent of copolymer composition. This size cut-off is likely an underestimate, as the method of calculating the dye sizes does not

Table 3
Chemical name, size, charge, and absorbance wavelength of small molecule probes used in the filtration experiments.

Solute name	Size (nm)	Charge	λ (nm)
Brilliant Blue R	1.11	−1	553
Direct Red 80	1.08	−6	528
Chicago Sky Blue 6B	0.88	−4	618
Acid Blue 45	0.84	−2	597
Ethyl Orange	0.82	−1	474
Methyl Orange	0.79	−1	479
Vitamin B12	1.3	0	361
Vitamin B2	0.85	0	445
Vitamin B6	0.72	0	324

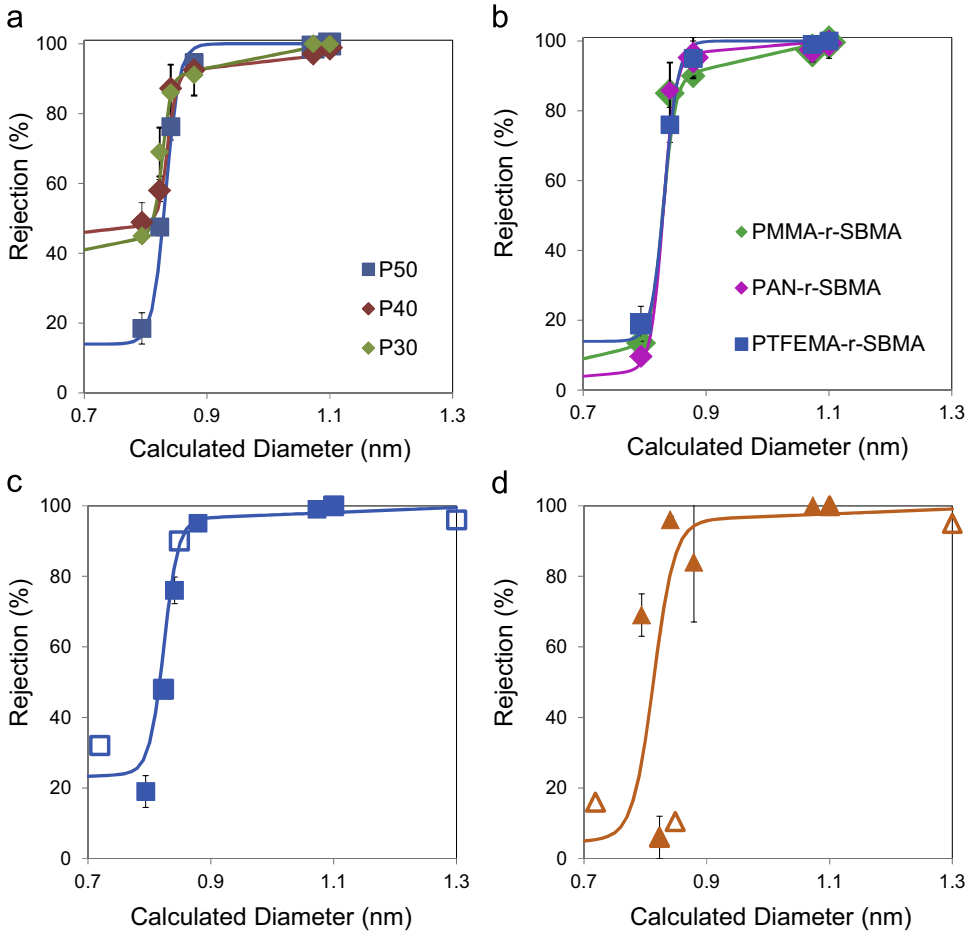

Fig. 6. Selectivity of TFC membranes with amphiphilic zwitterionic copolymer selective layers in comparison to a commercial membrane of similar pore size. a. Rejection of anionic dyes by PTFEMA-*r*-SBMA TFC membranes with varying SBMA contents. All three membranes show a sharp sized-based cut-off. Copolymer composition does not affect the size cut-off significantly. b. Rejection of anionic dyes by TFC membranes with selective layers of zwitterionic amphiphilic copolymers with three different hydrophobic components: PTFEMA-*r*-SBMA (P50), PMMA-*r*-SBMA, and PAN-*r*-SBMA. All membranes show essentially the same size cut-off, supporting the hypothesis that zwitterion self-assembly determines channel size and selectivity. (c,d) Rejections of charged (filled symbols) and neutral (empty symbols) dyes by c. P50 coated membrane and d. commercial PES 1 kDa membrane. Charged and neutral dyes roughly fit onto a single rejection curve (standard error of regression $S=5.12$) for the P50-coated membrane, demonstrating the selectivity is size-based, and not charge-based. In comparison, the commercial PES 1 kDa membrane shows a poor *S*-curve fit (standard error of regression $S=24.3$) and wide spread of rejections, indicating a lack of size-based selectivity. Error bars indicate maximum and minimum values for each data point.

take the hydration shell around the dyes into account. The channels are also partially filled with the zwitterionic groups, which can decrease the effective channel size. Hence, the dye filtration results are in close agreement with the nanochannel size ~1.2 nm measured with TEM. The fact that the size cut-off does not change with copolymer composition supports our hypothesis that the channel size is determined by the electrostatic interactions between the zwitterionic groups. It also demonstrates that changing the SBMA content affects the number of nanochannels, not the size. This further explains the differences in permeances between P50, P40 and P30-coated membranes. The fact that there is some permeability observed for P30 coated membranes, together with dye retention curves comparable with the other PTFEMA-*r*-SBMA coated membranes, indicates that a small number of zwitterionic domains indeed percolate through the thickness of this copolymer, at least when it is hydrated [67].

3.4.2.2. Effect of backbone chemistry. To test our hypothesis that channel size is determined by the zwitterionic group, we filtered the same dyes through the other two zwitterionic amphiphilic copolymers mentioned previously that were synthesized with SBMA contents in the monomer mixture comparable to P50. Fig. 6b shows the rejection curves for TFC membranes made with PAN-*r*-SBMA (52 wt% SBMA), PTFEMA-*r*-SBMA (47 wt% SBMA), and PMMA-*r*-SBMA (42 wt% SBMA) copolymers. The pure water permeances of these membranes were 1 ± 0.03 L m^{-2} h^{-1} bar^{-1}, 8.4 ± 0.35 L m^{-2} h^{-1} bar^{-1} and 10.7 ± 0.1 L m^{-2} h^{-1} bar^{-1}. These three membranes, whose selective layers are composed of copolymers with different hydrophobic backbone polymer but same zwitterion, have essentially the same size cut-off. This implies that the zwitterionic group determines the effective channel size and hence membrane selectivity.

3.4.2.3. Effect of solute charge. Fig. 6c and d shows the rejection of negatively charged and electrically neutral molecules. For the P50-coated membrane, charged and neutral solutes approximately fit onto a single rejection curve, especially at high rejections that are useful for most separations, with a standard error of regression *S* value of 5.12 which tells us the average distance of data points from the fitted line (Fig. 6c). This indicates that the selectivity of these new membranes is size-based and not strongly affected by solute charge. This is because the PTFEMA-*r*-SBMA copolymer is electrically neutral, so the selectivity of the membrane is driven not by electrostatic effects commonly seen in NF and RO membranes, but by size-based sieving.

In comparison, the commercial PES 1 kDa membrane shows a less consistent correlation between solute size and rejection (Fig. 6d). The fit of a typical *S*-curve to this data is poor, with a

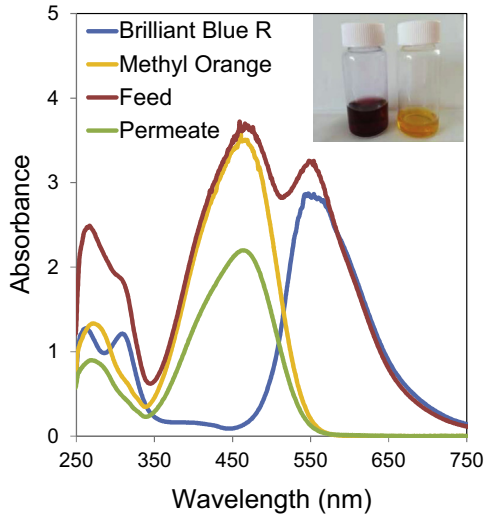

Fig. 7. Size-based small molecule separation capability of PTFEMA-*r*-SBMA TFC membranes. Two dye diafiltration experiment with a feed containing 50 ppm each of brilliant blue R (1.1 nm) and methyl orange (0.79 nm). Main image shows the UV spectra of the feed, permeate, and 50 ppm of each single dye for reference. Inset shows a photo of the feed (left) and the permeate (right). Only methyl orange permeates through the P50 TFC membrane, while brilliant blue was completely retained. (For interpretation of the references to color in this figure legend, the reader is referred to the web version of this article.)

standard error of regression *S* value of 24.3, since solute rejections deviate widely, especially right around the cut-off. Furthermore, rejections were observed to vary widely from swatch to swatch. This limits the ability to predict the applications in which the PES 1 kDa membrane can be used, as rejection depends on the particular solute, rather than only its size. Our membranes, on the other hand, demonstrate a sharp, size-based selectivity essentially independent of charge, unlike most commercial membranes including the one tested here.

3.5. Small molecule separation capability

To demonstrate the separation capability of our membranes, a solution containing 50 mg/L each of two negatively charged dyes, Brilliant Blue R (1.1 nm) and Methyl Orange (0.79 nm), was filtered through P50-coated TFC membrane. Fig. 7 shows the UV–visible spectra of each of these dyes, as well as the feed and permeate. The filtrate spectrum follows that of methyl orange at 70% of the initial concentration. The characteristic peak of Brilliant Blue R at 553 nm is not observed in the filtrate, indicating the dye was retained and separated completely.

3.6. Fouling resistance to model organic foulants

3.6.1. Protein (BSA) fouling

We tested the fouling resistance of PTFEMA-*r*-SBMA membranes with two representative feeds. Proteins are common foulants that show a strong tendency to adsorb on many surfaces, making them especially problematic. We used a solution of 1 g/L bovine serum albumin (BSA) in phosphate buffered saline (PBS). We found that the P50 copolymer showed some solubility in PBS, even though it was stable in deionized water. Zwitterionic polymers are known to “salt in” and become more soluble in saline solutions [34,38]. To prevent this issue, we performed this test on the P40-coated membrane, which was stable even at high salinity. BSA retention was $>99\%$, consistent with the reported globular dimensions of the protein (8 nm by 3 nm) [68] and the membrane pore size. Fig. 8a shows that during protein filtration, there is only a small decline in flux (7% over 24 h). The flux is fully recovered ($>99\%$) after rinsing the cell with DI water. The fluxes before and after are within error margins of each other. In comparison, the commercial 1 kDa PES membrane exhibited a flux decline of 41% which was not recovered after the water rinse.

3.6.2. Oil-in-water emulsion fouling

As a second foulant, we selected an oil-in-water emulsion. Large volumes of oily wastewaters are produced by oil and petroleum industry and their adequate disposal or treatment remains a big challenge [29]. We filtered a 1500 mg/L oil-in-water emulsion prepared using a 9:1 ratio of soybean oil to DC193 surfactant [62] for 50 h. The commercial PES 1 kDa membrane fouled rapidly and lost 88% of its permeance irreversibly (Fig. 8b). In comparison, the P50-coated TFC membrane exhibited exceptional fouling resistance. The flux declined only by 4% by the end of the experiment, and was completely recovered with a DI water rinse. The

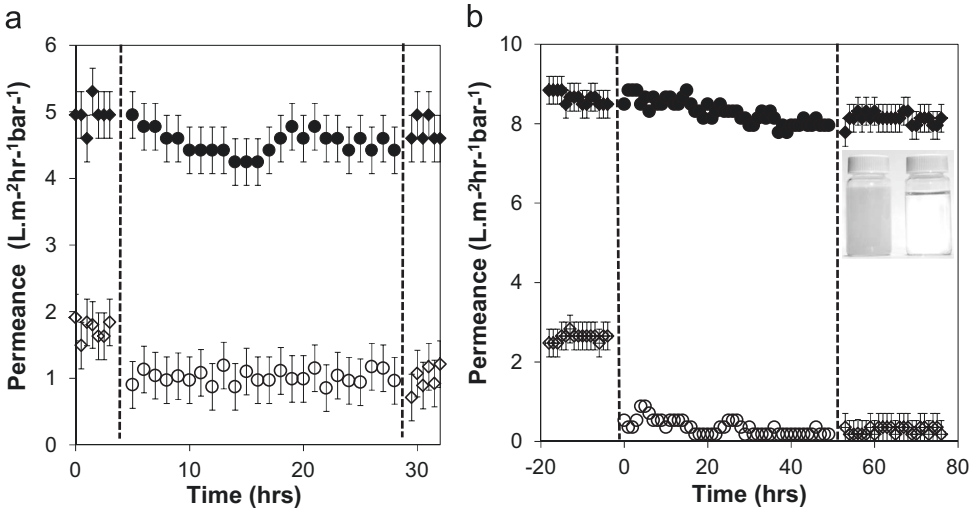

Fig. 8. Dead-end-filtration of foulant solutions through PTFEMA-*r*-SBMA TFC membranes (filled symbols) and a commercial membrane of similar pore size (empty symbols). Plots show the initial permeance of water (diamonds), followed by the permeance of the foulant solution (circles). Then, the membrane is rinsed with water several times, and water permeance is measured again (diamonds). In each case, PTFEMA-*r*-SBMA copolymer membranes show negligible flux loss during and after exposure to foulant solutions, whereas the commercial membrane shows significant irreversible flux loss. Error bars indicate limitations of measurement equipment. a. 1 g/L Bovine Serum Albumin in Phosphate Buffered Saline solution (P40-coated membrane, commercial PES 1 kDa). b. 1500 mg/L oil-in-water emulsion (P50-coated membrane, commercial PES 1 kDa). Inset shows a photo of the feed (left) that is gray in color and permeate (right) that appears clear, indicating retention of oil droplets components.

fluxes before and after are within error margins of each other.

These experiments show that this new class of membrane materials shows excellent fouling resistance, even with demanding feeds and in a dead-end configuration. Membrane permeances can be recovered with a water rinse to levels that are statistically indifferent from their initial value. In other words, these membranes resist irreversible, adsorptive fouling completely, at least for the time periods used in this study. This means that these membranes can be cleaned completely with a water rinse, obviating the use of cleaning chemicals and significantly extending membrane life. The fouling resistance mechanism of these membranes is likely associated with the high degree of hydration of the zwitterionic groups. Future studies will focus on better understanding the interaction between this class of membrane materials and common foulants, especially because this degree of fouling resistance is very rare, reported for only a few membrane materials [22,23,69].

3.7. Membrane stability and chlorine resistance

Zwitterionic materials are reported to show better chlorine resistance than PEO-based anti-fouling chemistries. To confirm this advantage, we tested the chlorine resistance of a P40-coated TFC membrane by soaking it in 1000 ppm sodium hypochlorite in water at a pH of 7.1 for 3 h. The pure water permeance was measured to be 6.34 ± 0.02 L m^{-2} h^{-1} bar^{-1} both before and after chlorine exposure, exhibiting no decline in flux after soaking. We also filtered a dye that is right around the size cut-off, Chicago Sky Blue 6B (0.88 nm). The dye retention showed no change within error margins, at 94 ± 0.7% before chlorine exposure and 95 ± 0.7% after. These results indicate excellent resistance to oxidative damage by chlorine.

4. Conclusions

This is, to our knowledge, the first time zwitterionic amphiphilic copolymers were used as membrane selective layers, and the first time the morphology of the self-assembly of such copolymers is shown by TEM. The data indicates a close correlation between the self-assembled nanostructure of the copolymer, and the performance of membranes whose selective layers they form. There is a close match between the effective size cut-off of the membranes and the zwitterionic domain size measured by TEM ($\sim$1.2 nm), indicating that the permeate passes through the network of zwitterion-filled, hydrophilic nanochannels. Solutes that cannot fit within these channels, the size of which is determined by the zwitterion structure, are retained regardless of their charge. Furthermore, their selectivity is sharp and size-based. These membranes exhibit high pure water permeabilities, significantly above the commercial membrane with comparable MWCO. They are also completely resistant to irreversible fouling within our measurements, showing negligible flux decline upon filtering an oil-in-water emulsion and a protein solution. The high flux, sharp selectivity, and exceptional fouling resistance of these membranes makes them promising for biomolecule separations, textile wastewater, and filtration of feeds with large fouling potential.

Acknowledgments

TEM was done utilizing the W.M.Keck foundation Biological Imaging Facility at the Whitehead Institute. Authors thank Dr. Nicki Watson at the Whitehead Institute for help with TEM data acquisition, Prof. Xiaobing Xu for access to DLS, and Prof. Meagan Mauter and Prof. Peggy Cebe for helpful discussions. Authors also thank Dr. Chiara Vannucci, Susan Colt, Akash Mittal, Lily Corcoran and David Wilbur for experimental help and useful discussions. This research was supported by Tufts University, and by the National Science Foundation (NSF) under Grant no. CBET-1437772.

References

[1] T. Burnouf, M. Radosevich, Nanofiltration of plasma-derived biopharmaceutical products, Haemophilia 9 (2003) 24–37.
[2] B. van der Bruggen, C. Vandecasteele, Removal of pollutants from surface water and groundwater by nanofiltration: overview of possible applications in the drinking water industry, Environ. Pollut. 122 (2003) 435–445.
[3] R.W. Baker, Membrane Technology and Applications, 2nd ed., J. Wiley, Chichester; New York, 2004.
[4] A. Asatekin, C. Vannucci, Self-assembled polymer nanostructures for liquid filtration membranes: a review, Nanosci. Nanotechnol. Lett. 7 (2015) 21–32.
[5] M.F.A. Goosen, S.S. Sablani, H. Ai-Hinai, S. Ai-Obeidani, R. Al-Belushi, D. Jackson, Fouling of reverse osmosis and ultrafiltration membranes: a critical review, Sep. Sci. Technol. 39 (2004) 2261–2297.
[6] M. Nystroem, L. Kaipia, S. Luque, Fouling and retention of nanofiltration membranes, J. Membr. Sci. 98 (1995) 249–262.
[7] S. Hong, M. Elimelech, Chemical and physical aspects of natural organic matter (NOM) fouling of nanofiltration membranes, J. Membr. Sci. 132 (1997) 159–181.
[8] R. van Reis, A. Zydney, Membrane separations in biotechnology, Curr. Opin. Biotechnol. 12 (2001) 208–211.
[9] A. Kalbasi, L. Cisneros-Zevallos, Fractionation of monomeric and polymeric anthocyainins from concord grape (*Vitis labrusca* L.) juice by membrane ultrafiltration, J. Agric. Food Chem. 55 (2007) 7036–7042.
[10] N. Hilal, O.O. Ogunbiyi, N.J. Miles, R. Nigmatullin, Methods employed for control of fouling in MF and UF membranes: a comprehensive review, Sep. Sci. Technol. 40 (2005).
[11] R.J. Petersen, J.E. Cadotte, Thin film composite reverse osmosis membranes, in: M.C. Porter (Ed.), Handbook of Industrial Membrane Technology, Noyes Publications, Park Ridge, NJ, 1990, pp. 307–348.
[12] K.B. Jirage, J.C. Hulteen, C.R. Martin, Nanotubule-based molecular-filtration membranes, Science 278 (1997) 655–658.
[13] K.F. Czaplewski, J.T. Hupp, R.Q. Snurr, Molecular squares as molecular sieves: size-selective transport through porous-membrane-supported thin-film materials, Adv. Mater. Commun. 13 (2001) 1895–1897.
[14] B.M. Carter, B.R. Wiesenauer, E.S. Hatakeyama, J.L. Barton, R.D. Noble, D.L. Gin, Glycerol-based bicontinuous cubic lyotropic liquid crystal monomer system for the fabrication of thin-film membranes with uniform nanopores, Chem. Mater. 24 (2012) 4005–4007.
[15] M. Zhou, T.J. Kidd, R.D. Noble, D.L. Gin, Supported lyotropic liquid-crystal polymer membranes: promising materials for molecular size-selective aqueous nanofiltration, Adv. Mater. 17 (2005) 1850–1853.
[16] D.L. Gin, G. Weiqiang, B.A. Pindzola, W.J. Zhou, Polymerized lyotropic liquid crystal assemblies for materials applications, Acc. Chem. Res. 34 (2001) 973–980.
[17] M. Zhou, P.R. Nemade, X. Lu, X. Zeng, E.S. Hatakeyama, R.D. Noble, D.L. Gin, New type of membrane material for water desalination based on a cross-linked bicontinuous cubic lyotropic liquid crystal assembly, J. Am. Chem. Soc. Commun. 129 (2007) 9574–9575.
[18] D.L. Gin, J.E. Bara, R.D. Noble, B.J. Elliott, Polymerized lyotropic liquid crystal assemblies for membrane applications, Macromol. Rapid Commun. 29 (2008) 367–389.
[19] E.S. Hatakeyama, C.J. Gabriel, B.R. Wiesenauer, J.L. Lohr, M. Zhou, R.D. Noble, D. L. Gin, Water filtration performance of a lyotropic liquid crystal polymer membrane with uniform, sub-1- nm pores, J. Membr. Sci. 366 (2011) 62–72.
[20] K.V. Peinemann, V. Abetz, P.F.W. Simon, Asymmetric superstructure formed in a block copolymer via phase separation, Nat. Mater. 6 (2007) 992–996.
[21] A. Asatekin, A.M. Mayes, Responsive pore size properties of composite NF membranes based on PVDF graft copolymers, Sep. Sci. Technol. 44 (2009) 3330–3345.
[22] A. Asatekin, A. Mennitti, S. Kang, M. Elimelech, E. Morgenroth, A.M. Mayes, Antifouling nanofiltration membranes for membrane bioreactors from self-assembling graft copolymers, J. Membr. Sci. 285 (2006) 81–89.
[23] A. Asatekin, E.A. Olivetti, A.M. Mayes, Fouling resistant, high flux nanofiltration membranes from polyacrylonitrile-graft-poly(ethylene oxide), J. Membr. Sci. 332 (2009) 6–12.
[24] A. Akthakul, R.F. Salinaro, A.M. Mayes, Antifouling polymer membranes with subnanometer size selectivity, Macromolecules 37 (2004) 7663–7668.
[25] S.Y. Yang, I. Ryu, H.Y. Kim, J.K. Kim, S.K. Jang, T.P. Russell, Nanoporous membranes with ultrahigh selectivity and flux for the filtration of viruses, Adv. Mater. 18 (2006) 709–712.
[26] S.P. Nunes, M. Karunakaran, N. Pradeep, A.R. Behzad, B. Hooghan, R. Sougrat, H.Z. He, K.V. Peinemann, From micelle supramolecular assemblies in selective solvents to isoporous membranes, Langmuir 27 (2011) 10184–10190.
[27] M.S.J. Ruokolainen, O. Ikkala, G. ten Brinke, E.L. Thomas, M. Torkkeli, R. Serimaa, Supramolecular routes to hierarchical structures: comb-coil

diblock copolymers organized with two length scales, Macromolecules 32 (1999) 1152–1158.
[28] A. Akthakul, A.I. Hochbaum, F. Stellacci, A.M. Mayes, Size fractionation of metal nanoparticles by membrane filtration, Adv. Mater. 17 (2005) 532–535.
[29] A. Asatekin, A.M. Mayes, Oil industry wastewater treatment with fouling resistant membranes containing amphiphilic comb copolymers, Environ. Sci. Technol. 43 (2009) 4487–4492.
[30] R.P. Lattimer, Mass spectral analysis of low-temperature pyrolysis products from poly(ethylene glycol), J. Anal. Appl. Pyrolysis 56 (2000) 61–78.
[31] K.J. Voorhees, S.F. Baugh, D.N. Stevenson, An investigation of the thermal degradation of poly(ethylene glycol), J. Anal. Appl. Pyrolysis 30 (1994) 47–57.
[32] E. Ostuni, R.G. Chapman, R.E. Holmlin, S. Takayama, G.M. Whitesides, A survey of structure–property relationships of surfaces that resist the adsorption of protein, Langmuir 17 (2001) 5605–5620.
[33] S.F. Chen, S.Y. Jiang, A new avenue to nonfouling materials, Adv. Mater. 20 (2008) 335–338.
[34] G.S. Georgiev, E.B. Karnenska, E.D. Vassileva, I.P. Kamenova, V.T. Georgieva, S. B. Iliev, I.A. Ivanov, Self-assembly, anti polyelectrolyte effect, and non-biofouling properties of polyzwitterions, Biomacromolecules 7 (2006) 1329–1334.
[35] R.E. Holmlin, X.X. Chen, R.G. Chapman, S. Takayama, G.M. Whitesides, Zwitterionic SAMs that resist nonspecific adsorption of protein from aqueous buffer, Langmuir 17 (2001) 2841–2850.
[36] J. Wu, W.F. Lin, Z. Wang, S.F. Chen, Y. Chang, Investigation of the hydration of nonfouling material poly(sulfobetaine methacrylate) by low-field nuclear magnetic resonance, Langmuir 28 (2012) 7436–7441.
[37] M. Herzberg, A. Sweity, M. Brami, Y. Kaufman, V. Freger, G. Oron, S. Belfer, R. Kasher, Surface properties and reduced biofouling of graft-copolymers that possess oppositely charged groups, Biomacromolecules 12 (2011) 1169–1177.
[38] Q. Yang, M. Ulbricht, Novel membrane adsorbers with grafted zwitterionic polymers synthesized by surface-initiated ATRP and their salt-modulated permeability and protein binding properties, Chem. Mater. 24 (2012) 2943–2951.
[39] Q. Li, Q.Y. Bi, B. Zhou, X.L. Wang, Zwitterionic sulfobetaine-grafted poly(vinylidene fluoride) membrane surface with stably anti-protein-fouling performance via a two-step surface polymerization, Appl. Surf. Sci. 258 (2012) 4707–4717.
[40] M.-Z. Li, J.-H. Li, X.-S. Shao, J. Miao, J.-B. Wang, Q.-Q. Zhang, X.-P. Xu, Grafting zwitterionic brush on the surface of PVDF membrane using physisorbed free radical grafting technique, J. Membr. Sci. 405–406 (2012) 141–148.
[41] M.M. Rohani, A.L. Zydney, Protein transport through zwitterionic ultrafiltration membranes, J. Membr. Sci. 397 (2012) 1–8.
[42] R. Yang, K.K. Gleason, Ultrathin antifouling coatings with stable surface zwitterionic functionality by initiated chemical vapor deposition (iCVD), Langmuir 28 (2012) 12266–12274.
[43] R. Yang, J.J. Xu, G. Ozaydin-Ince, S.Y. Wong, K.K. Gleason, Surface-tethered zwitterionic ultrathin antifouling coatings on reverse osmosis membranes by initiated chemical vapor deposition, Chem. Mater. 23 (2011) 1263–1272.
[44] W.W. Yue, H.J. Li, T. Xiang, H. Qin, S.D. Sun, C.S. Zhao, Grafting of zwitterion from polysulfone membrane via surface-initiated ATRP with enhanced antifouling property and biocompatibility, J. Membr. Sci. 446 (2013) 79–91.
[45] Q. Shi, Y.L. Su, W. Zhao, C. Li, Y.H. Hu, Z.Y. Jiang, S.P. Zhu, Zwitterionic polyethersulfone ultrafiltration membrane with superior antifouling property, J. Membr. Sci. 319 (2008) 271–278.
[46] Q. Sun, Y.L. Su, X.L. Ma, Y.Q. Wang, Z.Y. Jiang, Improved antifouling property of zwitterionic ultrafiltration membrane composed of acrylonitrile and sulfobetaine copolymer, J. Membr. Sci. 285 (2006) 299–305.
[47] G. Zhai, S.C. Toh, W.L. Tan, E.T. Kang, K.G. Neoh, C.C. Huang, D.J. Liaw, Poly (vinylidene fluoride) with grafted zwitterionic polymer side chains for electrolyte-responsive microfiltration membranes, Langmuir 19 (2003) 7030–7037.
[48] C. Zhou, X.L. Gao, S.S. Li, C.J. Gao, Fabrication and characterization of novel composite nanofiltration, membranes based on zwitterionic O-carboxymethyl chitosan, Desalination 317 (2013) 67–76.
[49] Y.-L. Ji, Q.-F. An, Q. Zhao, W.-D. Sun, K.-R. Lee, H.-L. Chen, C.-J. Gao, Novel composite nanofiltration membranes containing zwitterions with high permeate flux and improved anti-fouling performance, J. Membr. Sci. 390–391 (2012) 243–253.
[50] M. Galin, A. Chapoton, J.C. Galin, Dielectric increments, intercharge distances and conformation of quaternary ammonioalkylsulfonates and alkoxydicyanoethenolates in aqueous and trifluoroethanol solutions, J. Chem. Soc. Perkins Trans. 2 (1993) 545–553.
[51] J.L. Bredas, R.R. Chance, R. Silbey, Head head Interactions in zwitterionic associating polymers, Macromolecules 21 (1988) 1633–1639.
[52] M. Ehrmann, A. Mathis, B. Muerer, M. Scheer, J.C. Galin, Statistical n-butyl acrylate-(sulfopropy1)ammonium betaine copolymers. 2. Structural studies, Macromolecules 25 (1992) 2253–2261.
[53] M. Ehrmann, R. Muller, J.C. Galin, C.G. Bazuin, Statistical n-butyl acrylate-(sulfopropy1)ammonium betaine copolymers. 4. Dynamic mechanical properties, Macromolecules 26 (1993) 4910–4918.
[54] M. Ehrmann, J.C. Galin, B. Meurer, Statistical n-butyl acrylate-sulfopropyl betaine copolymers. 3. Domain size determination by solid-state NMR spectroscopy, Macromolecules 26 (1993) 988–993.
[55] Y.L. Zheng, M. Galin, J.C. Galin, Random ethylacrylate sulfonatopropylbetaine copolymers. 1. Synthesis and characterization, Polymer 29 (1988) 724–730.
[56] T.Y. Wu, F.L. Beyer, R.H. Brown, R.B. Moore, T.E. Long, Influence of zwitterions on thermomechanical properties and morphology of acrylic copolymers: implications for electroactive applications, Macromolecules 44 (2011) 8056–8063.
[57] A. Mathis, Y.L. Zheng, J.C. Galin, Random ethylacrylate zwitterionic copolymers: 3. Microphase separation as a function of the zwitterion structure, Polymer 32 (1991) 3080–3085.
[58] M. Ehrmann, J.C. Galin, Statistical n-butyl acrylate-sulfonato-propylbetaine copolymers: 1. Synthesis and molecular characterization, Polymer 33 (1991) 859–864.
[59] C.G. Bazuin, Y.L. Zheng, R. Muller, J.C. Galin, Random ethyl acrylatesulphonatopropylbetaine copolymers: 2. Dynamic mechanical properties, Polymer 30 (1989) 654–661.
[60] W. Schärtl, Light Scattering from Polymer Solutions and Nanoparticle Dispersions, 1 ed., Springer-Verlag, Berlin Heidelberg, 2007.
[61] Y. Song, E.E. Doomes, J. Prindle, R. Tittsworth, J. Hormes, C.S.S.R. Kumar, Investigations into sulfobetaine-stabilized Cu nanoparticle formation: toward development of a microfluidic synthesis, J. Phys. Chem. B 109 (2005) 9330–9338.
[62] R. Revanur, B. McCloskey, K. Breitenkamp, B.D. Freeman, T. Emrick, Reactive amphiphilic graft copolymer coatings applied to poly (vinylidene fluoride) ultrafiltration membranes, Macromolecules 40 (2007) 3624–3630.
[63] G. Odian, Principles of Polymerization, fourth ed., Wiley, New Jersey, 2004.
[64] M.A. Modestino, D.K. Paul, S. Dishari, S.A. Petrina, F.I. Allen, M.A. Hickner, K. Karan, R.A. Segalman, A.Z. Weber, Self-assembly and transport limitations in confined nafion films, Macromolecules 46 (2013) 867–873.
[65] K. Boussu, C. Vandecasteele, B. Van der Bruggen, Relation between membrane characteristics and performance in nanofiltration, J. Membr. Sci. 310 (2008) 51–65.
[66] H. Lee, R.M. Venable, A.D.J. Mackerell, R.W. Pastor, Molecular dynamics studies of polyethylene oxide and polyethylene glycol: hydrodynamic radius and shape anisotropy, Biophys. J. 95 (2008) 1590–1599.
[67] G.S. Hwang, D.Y. Parkinson, A. Kusoglu, A.A. MacDowell, A.Z. Weber, Understanding water uptake and transport in Nafion using X-ray microtomography, Acs Macro Lett. 2 (2013) 288–291.
[68] M.L. Ferrer, R. Duchosicz, B. Cassasco, J.G. de la Torre, A.U. Acuna, The conformation of serum albumin in solution: a combined phosphorescence depolarization-hydrodynamic modeling study, Biophys. J. 80 (2001) 2422–2430.
[69] A. Asatekin, S. Kang, M. Elimelech, A.M. Mayes, Anti-fouling ultrafiltration membranes containing polyacrylonitrile-graft-poly(ethylene oxide) as an additive, J. Membr. Sci. 298 (2007) 136–146.